Energy levels of bilayer graphene quantum dots

D. R. da Costa,[1,2,*] M. Zarenia,[2,†] Andrey Chaves,[1,3,‡] G. A. Farias,[1,§] and F. M. Peeters[2,1,‖]
[1]*Departamento de Física, Universidade Federal do Ceará, 60455-900 Fortaleza, Ceará, Brazil*
[2]*Department of Physics, University of Antwerp, Groenenborgerlaan 171, B-2020 Antwerp, Belgium*
[3]*Department of Chemistry, Columbia University, 3000 Broadway, New York, New York 10027, USA*
(Received 24 July 2015; published 23 September 2015)

Within a tight binding approach we investigate the energy levels of hexagonal and triangular bilayer graphene (BLG) quantum dots (QDs) with zigzag and armchair edges. We study AA- and AB- (Bernal) stacked BLG QDs and obtain the energy levels in both the absence and the presence of a perpendicular electric field (i.e., biased BLG QDs). Our results show that the size dependence of the energy levels is different from that of monolayer graphene QDs. The energy spectrum of AB-stacked BLG QDs with zigzag edges exhibits edge states which spread out into the opened energy gap in the presence of a perpendicular electric field. We found that the behavior of these edges states is different for the hexagonal and triangular geometries. In the case of AA-stacked BLG QDs, the electron and hole energy levels cross each other in both cases of armchair and zigzag edges as the dot size or the applied bias increases.

DOI: 10.1103/PhysRevB.92.115437 PACS number(s): 81.05.U−, 71.10.Pm, 03.65.Ta

I. INTRODUCTION

Since the first experimental realization of graphene [1], an atomically thin layer of carbon atoms, the study of quantum dots (QDs) in this material has been the subject of substantial theoretical [2] and experimental [3] works. Part of such intense interest results from suggestions that graphene quantum dots (GQDs) offer a promising host for spin qubits [4,5]. Because of the linear and gapless spectrum in graphene, the realization of GQDs using external gate potentials becomes very challenging. However, GQDs can be fabricated by direct etching of a graphene sheet into small flakes. In such QDs the shape and edges of the dot have very significant consequences on the electronic and transport properties [3,6,7]. For example, GQDs with zigzag edges exhibit a degenerate zero energy level in their spectrum, whereas the GQDs with armchair edges have an energy gap [8,9]. There exists several theoretical works pertinent to monolayer GQDs (with different geometries and different edges) in which the QD energy levels were studied using both tight-binding and continuum models [9,10]. Similar works on bilayer graphene (BLG) QDs are still very rare.

It has been recognized that AB-stacked BLG, i.e., two coupled layers of graphene, is a very different material from its monolayer [11]. The spectrum in AB-stacked pristine BLG is gapless and approximately parabolic at low energies. In the presence of a perpendicular electric field, however, the spectrum is found to display a gap, which can be tuned by varying the bias. Tailoring this tunable gap, using external gate potentials, has lead to the creation of electrostatically confined QDs in BLG [12,13]. The electronic properties of these QDs in BLG has been theoretically studied in both the absence and presence of external magnetic fields [14–18].

Similar to QDs made of monolayer graphene, one can consider small flakes in BLG as another type of QDs. In such QDs, the edges play an important role and modify strongly the energy spectrum. Despite the considerable number of theoretical studies in monolayer GQDs, similar studies in BLG are limited to triangular BLG flakes in zero magnetic field [19]. Systematic studies pertinent to BLG flakes with different geometries and different boundaries in the presence of a perpendicular electric field are, to our knowledge, absent.

In this paper, using the tight-binding (TB) approach, we obtain the energy levels of BLG QDs with triangular and hexagonal geometries in both the absence and presence of external electric fields. We study both AB- and AA-stacked BLG QDs with armchair and zigzag edges. We are able to describe approximately our numerical results for the energy spectra using a simplified continuum model and present analytical expressions for the size dependence of the energy levels.

Our paper is organized as follows. In Sec. II we briefly discuss the tight-binding approach used in our numerical calculations. In Secs. III and IV we present our results for the energy levels of the QDs with armchair and zigzag edges for AB- and AA-stacking BLG QDs, respectively. Finally, we present the concluding remarks in Sec. IV.

II. NUMERICAL METHOD

In order to describe electrons in BLG, we employ the tight-binding approach within the nearest-neighbor approximation. The Hamiltonian for BLG reads

$$H_{\mathrm{TB}} = \sum_{i\neq j}(\tau_{ij}c_i^{\dagger}c_j + \mathrm{H.c.}) + \sum_i V_i c_i^{\dagger}c_i, \qquad (1)$$

where c_i ($c_i^{\dagger}$) annihilates (creates) an electron in site i and τ_{ij} is the nearest neighbor hopping parameter. In AA-stacked BLG, the atoms in the upper and lower layer are located on top of each other, whereas in an AB-stacked BLG, the atoms in the A (B) sublattice in the bottom layer are linked with B (A) atoms in the top layer (i.e., the two monolayers are shifted with respect to each other). The hopping energy between the

*diego_rabelo@fisica.ufc.br
†mohammad.zarenia@uantwerpen.be
‡andrey@fisica.ufc.br
§gil@fisica.ufc.br
‖francois.peeters@uantwerpen.be

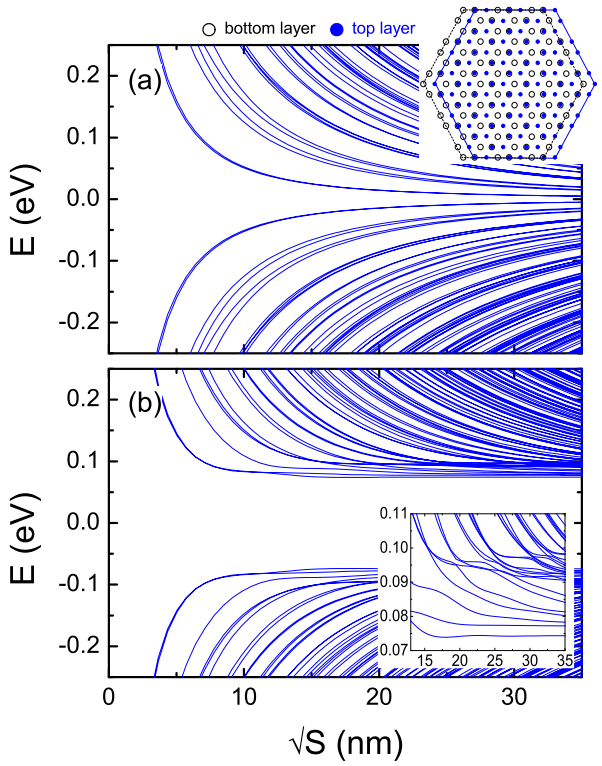

FIG. 1. (Color online) Energy levels (a) in the absence and (b) in the presence of bias potential ($V = 0.1$ eV) as a function of the square root of the dot area ($\sqrt{S}$), for hexagonal AB-stacked bilayer graphene quantum dots with armchair edges. A zoom around the lowest energy levels of the biased system is shown as an inset, in order to emphasize the lifting of the degeneracy of the states. The inset shows an AB-stacked armchair hexagonal BLG QD with $N = 3$ carbon hexagon at the edge.

atoms in the same layer is $t = -2.7$ eV, while the hopping for neighbor atoms stacked right on top of each other in different layers is $\tau_{AB} = -0.4$ eV (i.e., for the AB-stacked BLG QDs) and $\tau_{AA} = -0.2$ eV (i.e., for the AA-stacked BLG QDs). V_i is the on-site potential, which we take $V_i = V$ for the atoms in the upper layer and $V_i = -V$ for the atoms in the lower layer in the case of biased BLG QDs. Diagonalizing the matrix form of the Hamiltonian $H_{\rm TB}$, we obtain the energy levels of BLG QDs with different geometries. The evaluation of the density of states (DOS) is then performed by a superposition of individual energy states which we broaden using a Gaussian function $f(E) = \exp[-(E - E_0)^2/\Gamma^2]$, with a broadening factor Γ smaller than the energy levels separations. A broadening factor of $\Gamma = 0.0005$ eV is assumed in all figures from here onwards, unless otherwise stated.

III. AB-STACKED BILAYER GRAPHENE

A. Armchair edges

First, we consider the energy spectrum of AB-stacked BLG QDs with armchair edges. A schematic structure of the QD is shown in the inset of Fig. 1(a). Figures 1(a) and 1(b) show the energy levels of a hexagonal dot with armchair edges as function of the square root of the QD area ($\sqrt{S}$), respectively, for $V = 0$ and $V = 0.1$ eV. In the absence of bias [Fig. 1(a)] the energy levels decrease as $\sim 1/\sqrt{S}$. This behavior can be linked to the fact that the lowest energy bands in BLG follow the dispersion relation

$$E = \pm\left[V^2 + (\hbar v_F k)^2 + \frac{\tau_{AB}^2}{2} - \sqrt{\frac{\tau_{AB}^4}{4} + \left(4V^2 + \tau_{AB}^2\right)(\hbar v_F k)^2}\right]^{1/2}, \qquad (2)$$

with $v_F \approx 10^6$ m/s as the Fermi velocity. Assuming $k \propto n\pi/L$ (n is an integer) for a QD with the length size $L = \sqrt{2S/3\sqrt{3}}$ and for $V = 0$ we obtain $E \approx [(n\pi\hbar v_F/L)^2 + \frac{\tau_{AB}^2}{2} - \sqrt{\frac{\tau_{AB}^4}{4} + (n\pi\tau_{AB}\hbar v_F/L)^2}]^{1/2}$, which gives $E \approx \pm 1/L$ as $L \to \infty$. In the presence of a bias potential and for large L, one obtains $E \approx \pm[V - 2n\pi\hbar v_F/L^2]$ for the size dependence of the energy levels in a BLG QD. This explains why the lowest electron and hole states in the spectrum of Fig. 1(b) approach energies lower than the value of the applied potential V at large sizes of the QD. The anticrossings around $E \sim \pm V$ [see inset of Fig. 1(b)] are due to an interplay between edge states in the biased case, as we will demonstrate in what follows.

Figure 2 shows the density of states (DOS) and the electron probability densities corresponding to the first two energy levels of the spectra in Fig. 1 at $\sqrt{S} \approx 16.7$ nm ($L \approx 10.3$ nm). Our results show that the first two energy levels are degenerate for $V = 0$ (see blue curve) while this degeneracy breaks down when $V \neq 0$ (see red curve). In the absence of bias, the corresponding electron densities (see labels 1 and 2) in the lower $|\psi_1|^2$ and upper $|\psi_2|^2$ layers can be transformed into each other by a 180° rotation, which leads to the observed twofold degenerate state. This symmetry is brought by the layer symmetry of BLG when $V = 0$. For nonzero bias, such layer symmetry is broken, resulting in the lifting of the degeneracy of the first energy levels (see levels labeled by 3 and 4). In this case, the corresponding electron densities in panels 3 and 4 show that the electron is mostly confined around the same corner in each layer of the BLG hexagonal QD.

In Figs. 3(a) and 3(b) we show the energy levels of an armchair triangular QD in BLG as function of $\sqrt{S}$, with $S = \sqrt{3}L^2/4$ and L being the side length of the dot, respectively, for $V = 0$ and $V = 0.1$ eV. The triangular BLG QD structure with armchair edges is depicted in the inset of Fig. 3(a). Similarly to the spectra shown in Fig. 1 for the hexagonal BLG QDs, the energy spectrum of an armchair triangular QD in BLG exhibits a $1/\sqrt{S}$ dependence for $V = 0$ and $E \approx \pm[V - 2n\pi\hbar v_F/L^2]$ when $V = 0.1$ eV. Due to the triangular geometry, now the energy levels decrease as function of size in groups of 2, 4, 6, 8, ... states. This is more clear in the DOS plot shown in the lower panel of Fig. 4 for $\sqrt{S} = 16.726$ nm. The different groups of states are highlighted by different colors. The first (second) group of levels exhibit two (three) peaks in their total electron densities $|\psi_1|^2 + |\psi_2|^2$ and one (two) peak(s) in each layer (see panels 1, 2 for the first group and panels 3–6 for the second group of levels). Accordingly, one can expect four, five, ... peaks in the total electron density corresponding to the levels in the third, fourth, ... groups. This is reminiscent of the nodal character of the wave functions in quantum confined

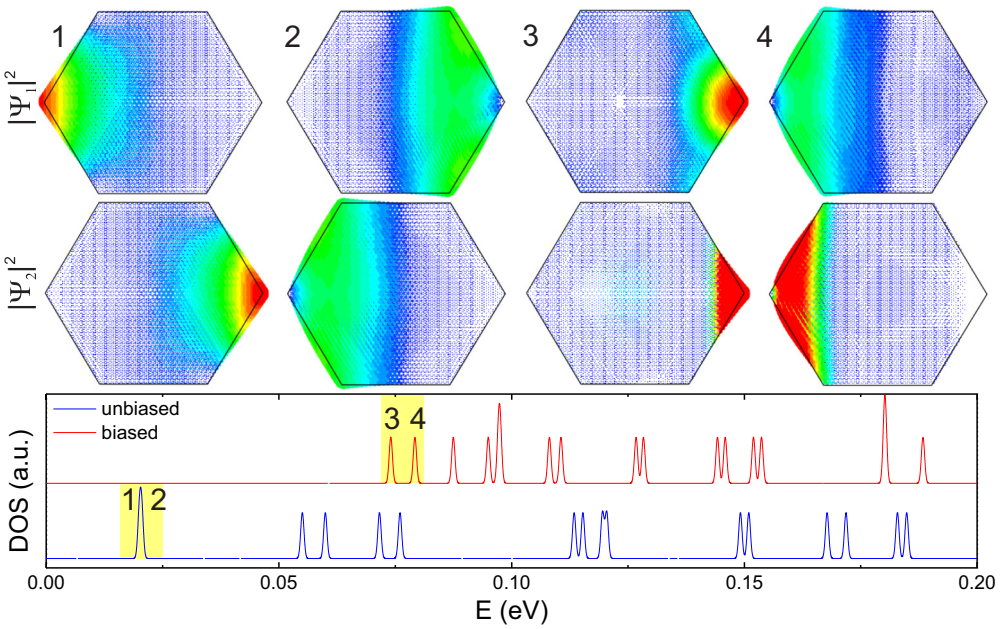

FIG. 2. (Color online) Density of states (bottom figure) of hexagonal AB-stacked bilayer graphene quantum dot with armchair edges in the absence (blue line) and the presence (red line) of a $V = 0.1$ eV electrostatic bias, for a dot with lateral size of $N = 25$ carbon rings ($L \approx 10.366$ nm which corresponds to $\sqrt{S} \approx 16.708$ nm). The probability density (upper figures) in the bottom ($|\Psi_1|^2$) and top graphene layers ($|\Psi_2|^2$) for the first two low-lying energy states are shown, namely, for points 1–2 and 3–4, respectively for the unbiased and biased cases. Red (blue) colors represent high (low) amplitude.

systems. In the absence of bias, the electron densities for the upper and lower layers can be transformed to each other by a reflection symmetry in the axis shown by the dashed line (compare upper and lower panels labeled by 1–6). Conversely, in the presence of bias, due to the breaking of the layer symmetry, this reflection symmetry is no longer present (see panels 7 and 8 for the first group of levels), which lifts the degeneracy of the first low-lying levels in the absence of the potential, as one can verify by comparing the peaks 1 and 2 (for unbiased case) with 7 and 8 (biased case) in the DOS plot.

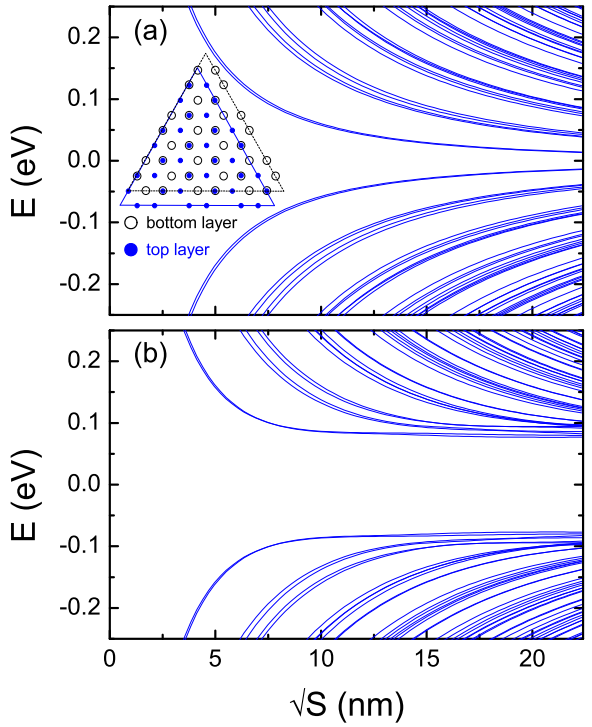

FIG. 3. (Color online) The same as Fig. 1, but now for armchair triangular AB-stacked bilayer quantum dots.

B. Zigzag edges

Figures 5(a) and 5(b) show the energy levels of a hexagonal BLG QD with zigzag edges, respectively, for $V = 0$ and $V = 0.1$ eV. In the absence of bias, as the QD size increases, the energy levels quickly converge to zero and a degenerate zero-energy level appears. This zero energy level is an *edge state*, which is due to the zigzag atoms at the edges in both layers of the BLG QD. The inset of Fig. 5(a) shows the first energy level as function of L (the side length of the hexagonal BLG QD), which is well fitted to $E = \alpha(1/L^{\beta})$ (red solid curve), where $\alpha = 610.4$ and $\beta = 3$ are fitting parameters. In the case of nonzero bias, edge states appear in the energy window $|E| \leqslant 0.1$ eV and a mini gap opens between the electron and hole edge states. Remarkably, the edges states display an oscillatory behavior as function of the size of the QD. Besides, those states for which the electrons are mainly confined at the zigzag edges of the upper (lower) layer approach $E = +V$ ($E = -V$). To provide a better understanding of the behavior of the energy levels in the presence of these edge states, we show in Fig. 6 the energy of the first electronic edge state and the corresponding total electron densities for $N = 8,9,\ldots,15$, where N is the number of zigzag atoms at each edge of the hexagonal QD. The total probability density plots in Fig. 6(c) demonstrate that: First, the electrons are confined mainly along the edges for which the terminated atoms are not linked to the other

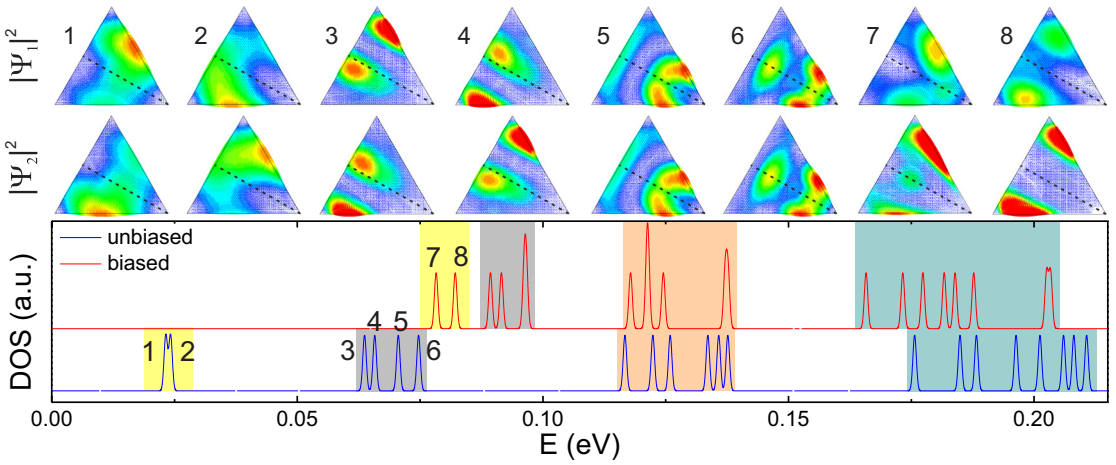

FIG. 4. (Color online) The same as Fig. 2, but now for an armchair triangular AB-stacked bilayer quantum dot with lateral size of $N = 60$ carbon rings ($L \approx 25.418$ nm and $\sqrt{S} \approx 16.726$ nm). The probability density for the bottom ($|\Psi_1|^2$) and top layers ($|\Psi_2|^2$) are shown for points 1–6 and 7–8, respectively, for the unbiased and biased cases. The different colors on the background of the density of states accentuate the set of states belonging to the same branch.

layer via the interlayer hopping term [see the structure of a zigzag hexagonal BLG flake with $N = 3$ in Fig. 6(a), for better clarification]. Second, the electrons are mainly confined along the edges of the lower layer for the edge states whose energy decrease with the dots lateral size, i.e., $N = 8,9,12,13$, whereas they are confined at the edges of the upper layer for those whose energy increase with size (see electron densities for $N = 10,11,14,15$).

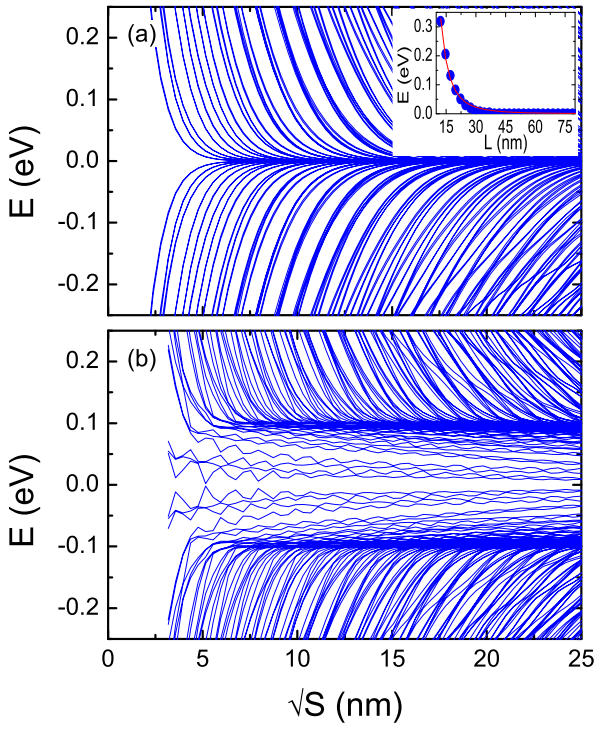

FIG. 5. (Color online) Energy levels (a) in the absence and (b) in the presence of a $V = 0.1$ eV bias potential as a function of the square root of the dot area ($\sqrt{S}$), for hexagonal AB-stacked bilayer graphene quantum dots with zigzag edges. The inset shows the trend of the first energy level, that exhibits a $1/L^3$ behavior, as verified by the fitting function (red solid line).

The energy levels of a triangular BLG QD with zigzag edges are shown in Figs. 7(a) and 7(b), respectively, for $V = 0$ and $V = 0.1$ eV. In the absence of bias, the energy spectrum exhibits a zero energy level, with $2(N-1)$ degenerate states, namely, $N-1$ zero states for each triangular layer, where N is the number of carbon atoms in each side of the QD. The higher energy levels are doubly degenerate and decay as a function of the size with a $1/L$ dependence, similar to that of triangular BLG QDs with armchair edges. Notice that the twofold degeneracy of the higher energy levels is not related to the layer symmetry of the BLG flake, but rather to the triangular symmetry of the QD, as observed before in triangular monolayer GQDs with zigzag edges [9]. In the presence of bias, the $2(N-1)$ degenerate zero energy states split into two groups of edge states: (i) $N-1$ degenerate states with energy $E = -0.1$ eV, that are confined at the edges of the lower layer, which, indeed, is at a -0.1 eV potential. These are reminiscent of edge states in a triangular monolayer graphene flake [9]. (ii) The other $N-1$ states stem from the $E = 0.1$ eV level and spread into the energy gap $|E| \leqslant V$, yet remaining twofold degenerate. The asymmetry of the spectrum for $V \neq 0$ is a consequence of the different structure of the edge atoms in the upper and lower layers of the triangular BLG QDs [see the inset of Fig. 7(a)]. This is in contrast with the hexagonal geometry of BLG QDs [Fig. 6(a)] in which both layers display the same structure for edge atoms.

Figures 8 and 9 show the DOS and the electron density corresponding to the lowest electronic states of the spectra shown, respectively, in Fig. 7(a) (for zero bias) and Fig. 7(b) (with $V = 0.1$ eV), for a QD size of $\sqrt{S} \approx 16.7$ nm. In the absence of bias, the total probability density corresponding to the Nth zero-energy state (see panel 1) indicates that the carriers are strongly confined at the edges, as expected. As we move to higher energy levels, the confinement is mostly inside the QD, exhibiting the nodal character of localized states (see panels 2–7). Similar to the energy spectrum of armchair triangular BLG QDs (Fig. 3), the nonzero energy levels of

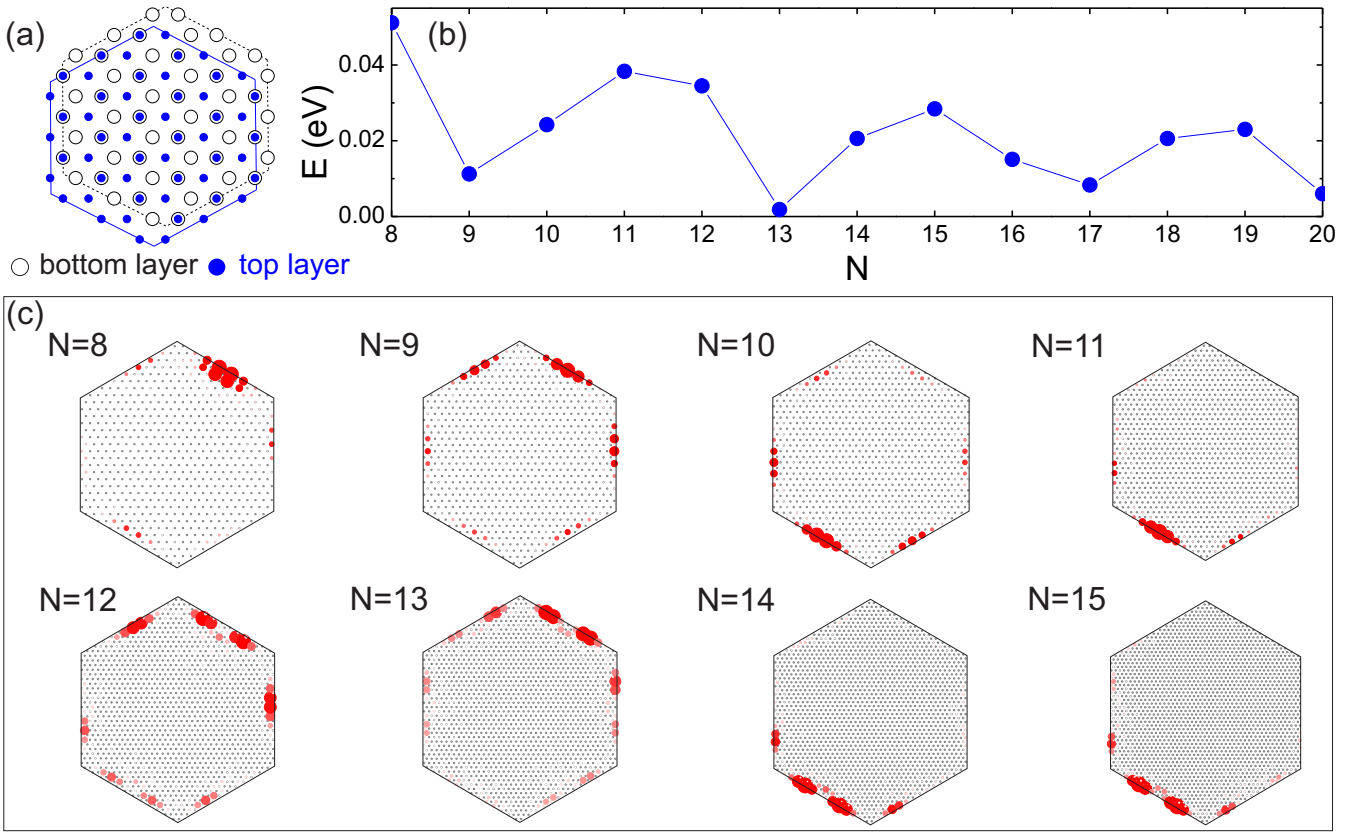

FIG. 6. (Color online) (a) A bilayer structure with $N = 3$ carbon rings of size is shown to demonstrate the edge terminations in zigzag hexagonal BLG QDs and the shift of the top layer with respect to the bottom layer due to the AB stacking. The atoms of the bottom (top) layer are represented by open black (blue closed) symbols. (b) Ground state energy in the biased dot spectrum for $V = 0.1$ eV [see Fig. 5(b)] as a function of the number of carbon rings N on one side of the hexagonal dot. (c) The total probability density for the ground state of a zigzag hexagonal quantum dot with $N = 8$–15 carbon rings in each of its sides. Notice that the group of states with $N = 8,9,12,13$ and $N = 10,11,14,15$ presents the same wave function symmetry.

zigzag triangular QDs decay as a function of size in groups of 2,4,6, . . . states (notice that all peaks for nonzero energy levels are doubly degenerate), and those states in the same group exhibit the same number of peaks in their total probability density, differing only in the spatial distribution of the peaks. For the biased case, the probability density of the $E = -0.1$ eV states, illustrated in panel 1 of Fig. 9, confirms that these are edge states of the lower layer, as previously suggested. Higher energy states inside the $|E| < 0.1$ eV gap are shown to be also edge states, but with a number of nodes that increase with the state energy level. These are reminiscent of quantum well states along the edges—indeed, by increasing $\sqrt{S}$, one effectively increases the edge size L (or, analogously, the width of the quantum well along the edge) and, consequently, the energies of all edge confined states must decrease, as shown in Fig. 7(b).

Since the states inside the energy gap appear only for gated zigzag hexagonal and triangular BLG QDs, it is interesting to investigate how the energy spectra of these systems depend on the applied gate potential, which is shown, respectively, in Figs. 10(a) and 10(b), for $\sqrt{S} \approx 16$ nm. As mentioned before, the electron and hole levels are symmetric (asymmetric) in hexagonal (triangular) QDs, due to the symmetric (asymmetric) structure of the zigzag edges in the upper and lower layers. In contrast to triangular BLG QDs, the energy spectrum of hexagonal BLG QDs exhibit anticrossings in both $|E| \leqslant V$ and $|E| > V$ regions. The nature of the anticrossings in the $|E| \leqslant V$ region is the same as the one for those observed in Fig. 5(b), which were due to an interplay between electron states localized in the nonconnected zigzag edges of the upper and lower layers. On the other hand, anticrossings in the $|E| > V$ region are due to the overlap between the edge states localized at the *corners* of the hexagonal QD, as one can verify from Fig. 10(c) by the bottom $|\Psi_1|^2$ and top $|\Psi_2|^2$ electron probability densities for the energies around the highlighted anticrossing in Fig. 10(a), whose states are labeled as 1–4 in the spectrum at $V = 0.025$ eV. The electron densities corresponding to these corner-localized edge states show electron confinement on the zigzag corner atoms that are on top of each other (i.e., A sublattice in one layer and B sublattice in the other). The wave functions for the 1 and 4 states, which are away from the anticrossing, share similarities, namely, the contribution from the bottom and top layers are asymmetric, exhibiting peaks only at the upper-right and lower-left corners, respectively, so that the total wave function distribution (summing both layer contributions) shows peaks in all six corners of the hexagonal dot. Conversely, for states 2 and 3, both layers contribute with wave functions localized

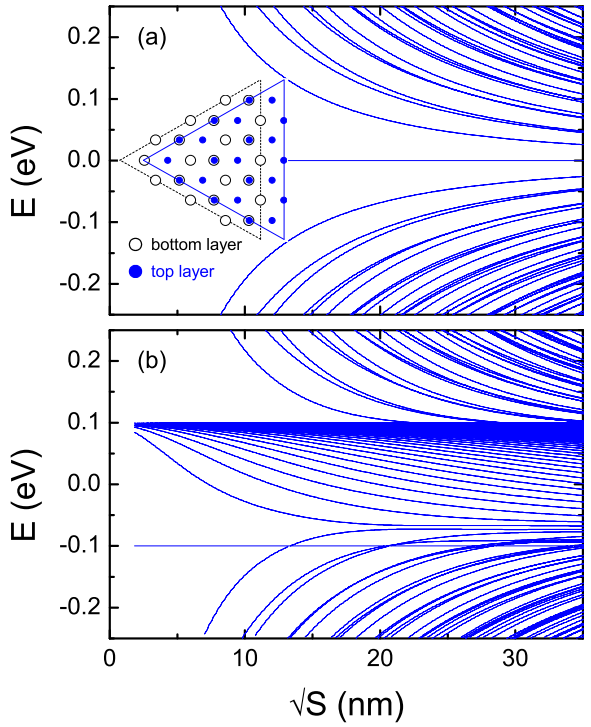

FIG. 7. (Color online) The same as Fig. 5, but now for zigzag triangular AB-stacked bilayer quantum dots. A sketch of the triangular structure is shown in the inset for $N = 3$ carbon rings at each size, where open black (closed blue) symbols correspond to the carbon atoms in bottom (upper) layer.

in the same corners, leading to a total wave function that is localized only at one side of the hexagon, as a manifestation of the in-plane asymmetry of the edges in the system.

IV. AA STACKED BILAYER GRAPHENE

Several properties discussed in the previous section are demonstrated to be related to interlayer asymmetry. Therefore, it is interesting to make a comparative study to a more symmetrical lattice structure. In order to do so, we investigate now the energy levels for bilayer graphene quantum dots formed by a layer stacking of the AA type, whose bottom and top layers are exactly on the top of each other.

A. Armchair edges

Figure 11 depicts the density of states as a function of the square root of the dot area ($\sqrt{S}$) for (a) hexagonal and (b) triangular BLG QDs with armchair edges. In the insets of Figs. 11(a) and 11(b) we show the AA-stacked hexagonal and triangular QDs sketches, respectively. Both spectra exhibit similar behavior: the two branches composed by positive and negative low energies cross each other at the zero-energy axis, thus preserving the electron-hole symmetry $E_e = -E_h$. These spectra are different from those of armchair AB-stacked BLG QD, where a clear energy gap is observed for any dot size. To understand better the behavior of these spectra, let us consider the four-band Hamiltonian within the continuum model for a AA-stacked bilayer graphene sheet [20,21]. For the K valley this Hamiltonian can be expressed as follows:

$$H = \begin{pmatrix} V_1 & \hbar v_F \pi & \tau_{AA} & 0 \\ \hbar v_F \pi^\dagger & V_1 & 0 & \tau_{AA} \\ \tau_{AA} & 0 & V_2 & \hbar v_F \pi^\dagger \\ 0 & \tau_{AA} & \hbar v_F \pi & V_2 \end{pmatrix}, \quad (3)$$

where $\pi = k_x + ik_y = ke^{i\theta_k}$ and $\pi^\dagger = k_x - ik_y = ke^{-i\theta_k}$ are the momentum operators with $\theta_k = \tan^{-1}(k_x/k_y)$, and $V_{1,(2)} = V(-V)$ is the electrostatic potential at the two layers. The eigenstates of the Hamiltonian (3) are given by the four-component wave function $\Psi = [\psi_A, \psi_B, \psi_{A'}, \psi_{B'}]^T$. Diagonalizing Eq. (3) and assuming $k = n\pi/L$, with $n \in \mathcal{Z}$ and L is the dot size, we obtain the eigenenergy spectrum

$$E = \pm\left[\frac{\hbar v_F n\pi}{L} \pm \sqrt{V^2 + \tau_{AA}^2}\right]. \quad (4)$$

Based on this formulation, we plot the energy levels as function of the length size L for n in the range [0,5] in Fig. 11(c). It is clear that the tight-binding spectra for the armchair hexagonal and triangular quantum dots, shown, respectively, in Figs. 11(a) and 11(b), are qualitatively similar to the one obtained analytically, by using the 4×4 Hamiltonian Eq. (3) within the continuum model, shown in Fig. 11(c). In fact, our results show that the AA-stacked BLG spectra for QDs with armchair edges: (i) decrease with the dot size as $1/L$ or, equivalently, $1/\sqrt{S}$, and (ii) that the AA bilayer sheet spectra are just a superposition of two single layer graphene spectra shifted up and down by $\pm\tau_{AA}$. Actually, for a more general $V \neq 0$, according to the analytical expression Eq. (4), it is clear that, from the four bands of the system, two energy sets (the higher electron band and the lower hole band) converge to $E = +\sqrt{V^2 + \tau_{AA}^2}$, whereas the other two sets approach $E = -\sqrt{V^2 + \tau_{AA}^2}$ (the lower electron band and the higher hole band)—these values correspond to the energies of the two doubly degenerate $n = 0$ states, shown as black solid lines in Fig. 11(c). Notice also that sets of states are formed for the triangular dot [Fig. 11(b)], just like those observed in the AB-stacked situation shown in Fig. 3. The main difference between the branches for the former [Fig. 11(b)] and the latter [Fig. 3(a)] is in the fact that the energy gaps that separate the branches of states are larger for AB stacking as compared to AA stacking. Besides, for the AA-stacking case, not all states are nondegenerate, as is evident for the AB-stacking configuration.

B. Zigzag edges

Figures 12(a) and 12(b) show the density of states and energy levels, respectively, for AA-stacked hexagonal and triangular BLG QDs with zigzag edges as function of the QD size $\sqrt{S}$ for zero bias potential. Schematic structures of these AA-stacked QDs with zigzag edges are illustrated in the inset of Figs. 12(a) and 12(b). In addition to the bulk localized states, which follow the analytical expression Eq. (4), the energy spectrum of hexagonal QDs exhibits several edges states that spread out in the range of $|E| \leqslant \tau_{AA}$. The energy levels of AA-stacked triangular dots [Fig. 12(b)] suggests that this difference between the spectra of hexagonal and triangular geometries is a consequence of the fact that all

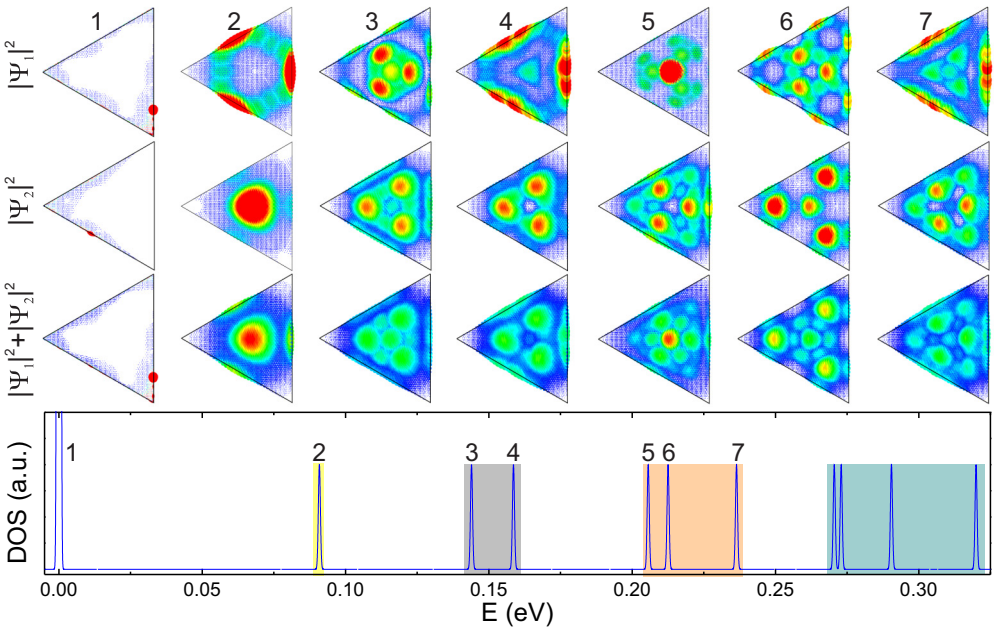

FIG. 8. (Color online) Density of states of a zigzag triangular AB-stacked bilayer graphene quantum dot, in the absence of an electrostatic bias, with $N = 103$ carbon rings in each of its sides, which corresponds to $L \approx 25.415$ nm and $\sqrt{S} \approx 16.724$ nm [see Fig. 7(a)]. The probability density for each layer (bottom $|\Psi_1|^2$ and top $|\Psi_2|^2$ layer amplitudes), as well as the total contribution ($|\Psi_1|^2 + |\Psi_2|^2$) are shown for points 1 (zero-energy level) and 2–7 (three first positive energy groups of states of the spectrum). The different colors on the background of the density of states plot illustrate the set of states belonging to the same branch, formed by 2, 4, 6, and 8 states. As all states are twofold degenerate, only 1, 2, 3, and 4 peaks are visible in these energy sets, respectively. Red (blue) colors represent high (low) amplitude of the wave function.

edge atoms in a AA-stacked triangular BLG QD terminate to the same sublattice, while for a hexagonal QD the adjacent lengths terminate to the different sublattices. Furthermore, the spectrum for the triangular case in Fig. 12(b) exhibits two straight horizontal states as the dot size increases, located at the energies $E = \pm\sqrt{V^2 + \tau_{AA}^2}_{=\pm\tau_{AA}=\pm 0.2}$ eV. These dot size independent states are not present in the armchair case (Fig. 11), but they are also observed in the analytical spectrum shown in Fig. 11(c) and they correspond to energy values for $n = 0$, as previously mentioned. Besides, just like in the analytical case, these two levels as obtained by using the tight-binding model are also degenerate. In the latter they are $(N-1)$-fold degenerate, while the analytical ones are just twofold degenerate. Comparing the spectra for the triangular zigzag case in the two different arrangements, AA and AB, respectively shown in Figs. 12(b) and 7(a), one can infer, by analogy, that these levels are actually edge states, which explains why they appear only in case of zigzag edges.

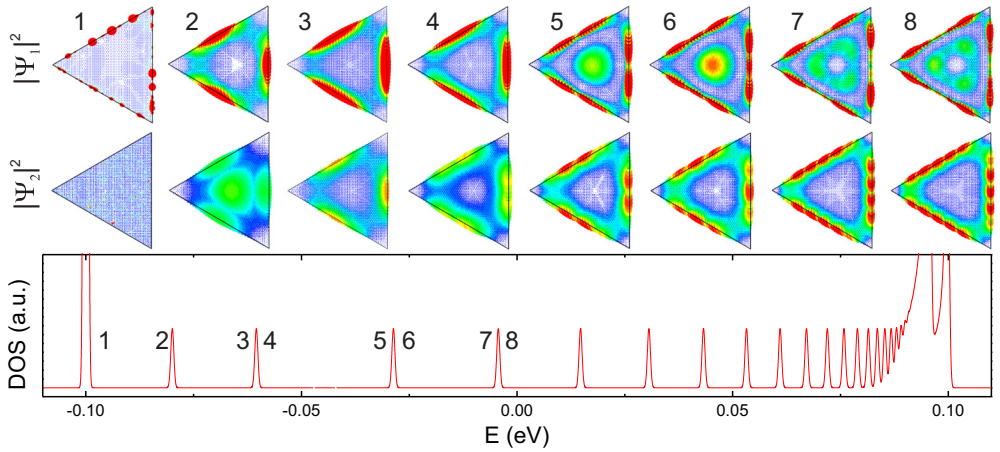

FIG. 9. (Color online) Density of states of a zigzag triangular AB-stacked bilayer graphene quantum dot, in the presence of a $V = 0.1$ eV electrostatic bias, with $N = 103$ carbon rings in each of its sides, which corresponds to $L \approx 25.415$ nm and $\sqrt{S} \approx 16.724$ nm [see Fig. 7(b)]. The probability density contributions for each layer (bottom $|\Psi_1|^2$ and top $|\Psi_2|^2$ layer amplitudes) are shown for points 1 [a $E = -V$ energy state formed by $(N-1)$ degenerated levels, energetically close to point 2], 2 (state that belongs to the negative branch of states in the spectrum), and 3–8 (edge states). Red (blue) colors represent high (low) amplitude of the wave function.

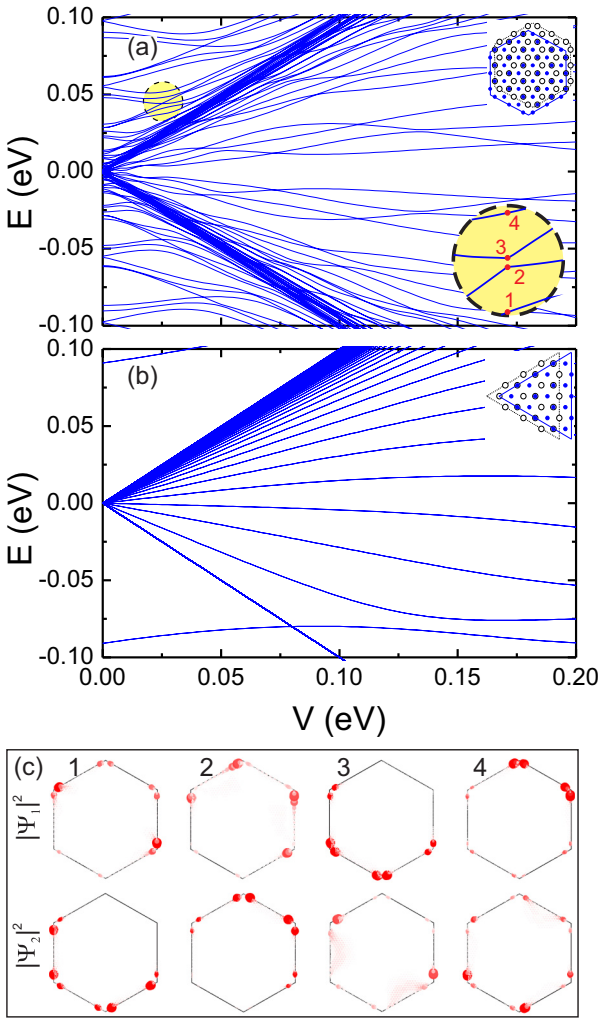

FIG. 10. (Color online) Energy levels as a function of the bias potential V for (a) hexagonal (with $N = 41$ carbon rings in each side, which corresponds to $L \approx 10.084$ nm and $\sqrt{S} \approx 16.254$ nm) and (b) triangular (with $N = 103$ carbon rings in each side, which corresponds to $L \approx 25.415$ nm and $\sqrt{S} \approx 16.724$ nm) AB-stacked BLG QDs with zigzag edges. The QD structures are illustrated in the insets. (c) The probability amplitude for the bottom $|\Psi_1|^2$ and top $|\Psi_2|^2$ layers are shown for points 1–4 [see inset of Fig. 10(a)] with $V = 0.025$ eV, which helps to understand the origin of the anticrossings observed in the spectrum for $|E| \gtrsim V$.

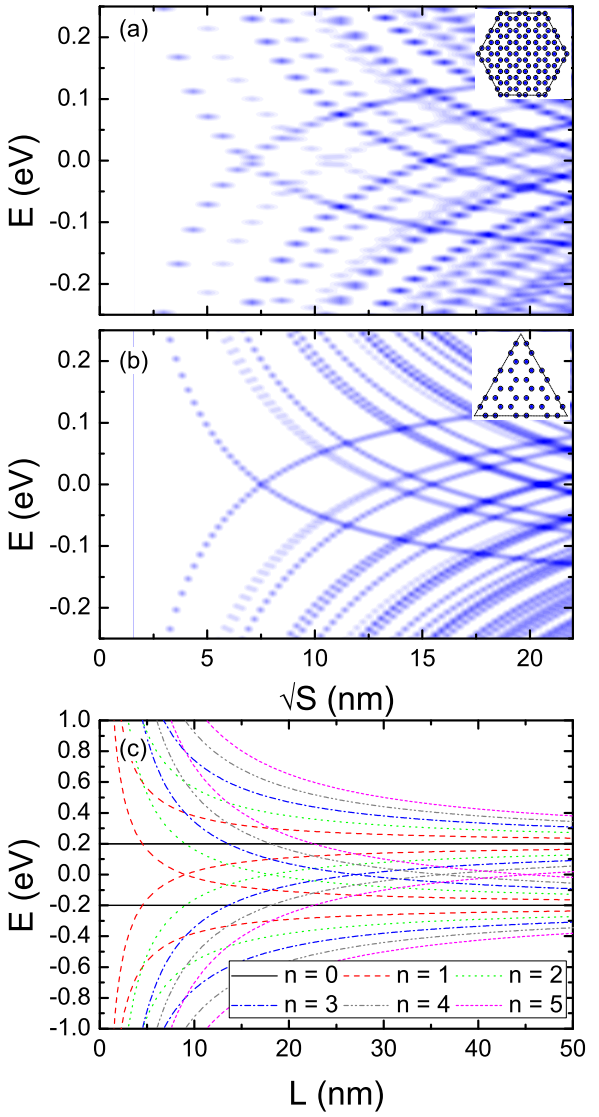

FIG. 11. (Color online) Density of states in the absence of bias potential as a function of the square root of the dot area ($\sqrt{S}$) for (a) hexagonal and (b) triangular AA-stacked BLG QD with armchair edges. The QD structures are illustrated in the insets. A broadening factor of $\Gamma = 0.005$ eV was considered for the Gaussian distribution of the DOS. Dark (light) blue color represents high (low) degeneracy of the energy levels. (c) Analytical energy levels [Eq. (4)] as obtained from the continuum bilayer graphene Hamiltonian as a function of size $L = n\pi/k$ in the absence of bias potential for $n \in [0,5]$.

In addition, both AB- and AA-stacked triangular dots exhibit the formation of energy minibands, shown respectively in Figs. 7(a) and 12(b). These sets of energy levels in the AA-stacked case are also double degenerate and decrease as a function of the system size in groups of even numbers 2, 4, 6, 8, ... This is illustrated in Fig. 13, where we plot the density of states of a AA-stacked triangular dot, emphasizing by different background colors the set of states belonging to the same energy branch. The total probability densities ($|\Psi_1|^2 + |\Psi_2|^2$) for the first three branches are shown by the points 1, 2–3, and 4–6. Comparing Figs. 8 and 13, one realizes that the total probability density for the states obtained for the triangular QDs with AA stacking have the same behavior, symmetry, number, and position of peaks as those for the BLG QDs with AB stacking: the states 1, 2–3, 4–6 in Fig. 13 correspond to the 2, 3–4, 5–7 states in Fig. 8. The only difference between the wave functions for these two kinds of stackings for zigzag triangular BLG QDs is that for AA stacking, both top and bottom probability densities have the same contributions, i.e., $|\Psi_1|^2 = |\Psi_2|^2$, due to the interlayer symmetry.

The dependence of the energy spectrum of the AA-stacked BLG QDs on the bias potential V is depicted in Fig. 14(a), for the hexagonal geometry, and Fig. 14(b), for the triangular geometry. Results are shown for quantum dots with zigzag edges, but those for armchair edges are qualitatively similar. In contrast to the AB-stacked case, the spectra for AA-stacked

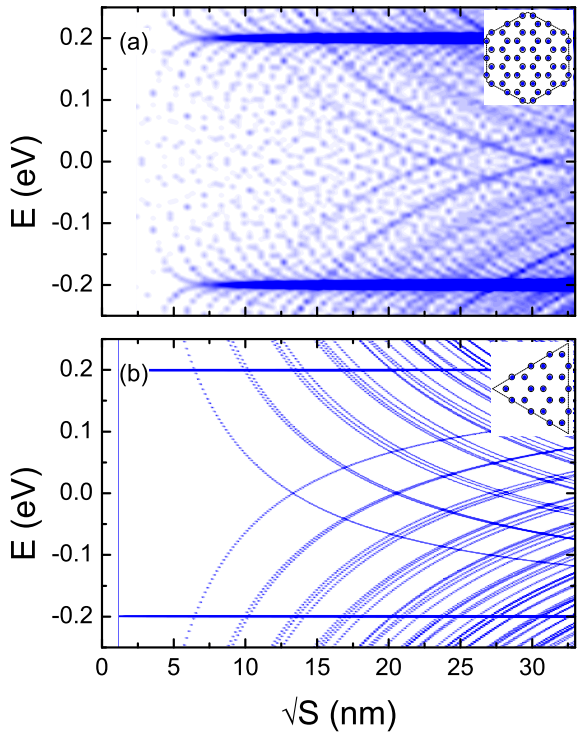

FIG. 12. (Color online) Density of states in the absence of bias potential as a function of the square root of the dot area ($\sqrt{S}$) for (a) hexagonal and (b) triangular AA-stacked BLG QDs with zigzag edges. The QD structures are illustrated in the insets. Broadening factors $\Gamma = 0.005$ eV and $\Gamma = 0.001$ eV are considered for the Gaussian distribution of the DOS in (a) and (b), respectively. Dark (light) blue color represents high (low) degeneracy of the energy levels.

biased armchair BLG QD do not exhibit a bias induced energy gap. Energy levels obtained by the tight-binding model in all cases follow qualitatively the trends predicted by the analytic expression Eq. (4), as shown in Fig. 14(c), such that both spectra exhibit crossings between states with different quantum numbers n. The crossings of the energy levels as a function of the bias potential have been already reported in the literature for the bilayer sheet in Ref. [20] and are easily verified by Eq. (4). Our analytical approximation proofs to be a reasonable model, providing good agreement with tight-binding results for both kinds of edges of quantum dots with a AA stacking, even in the presence of bias. All states for different n's cross each other once, except for the (twofold degenerate) $n = 0$ states. Notice that for both zigzag and armchair QDs with AA stacking, the energy spectra are symmetric with respect to $E = 0$, even in the presence of bias. Such symmetry is not observed in the Bernal stacking case: the spectrum for triangular zigzag QDs, shown in Figs. 7(b) and 10(b), is clearly asymmetric with respect to $E = 0$ in the presence of bias. This lends support to our previous conclusion that the electron-hole asymmetry in those spectra are due to the layers asymmetry of the AB-stacked structure, which, indeed, is not present in the AA-stacking case. Due to the electron-hole symmetry of the energy spectrum in the present case, the levels with the same index n cross each other at energy $E = 0$, whereas states with different values of n cross each other at different energies.

A deeper analysis on the energy spectrum as a function of the dot size in the presence of bias, as we made for AB-stacked dots in Figs. 1(b), 3(b), 5(b), and 7(b), is omitted here, since in the AA-stacked case, the energy difference between the biased and unbiased cases did not turn out to be as large as that found for AB-stacked dots, for such small values of bias potential V considered in this work, which simply yields small shifts in the energy levels. For instance, for $n = 0$ in Eq. (4) the energy value for $V = 0.1$ eV is $E \approx \pm 0.2236$ eV, while it is $E = \pm 0.2$ eV for $V = 0$.

V. CONCLUSION

Within the tight-binding approach we obtained the energy levels of bilayer graphene quantum dots both in the absence and in the presence of a perpendicular electric field. We

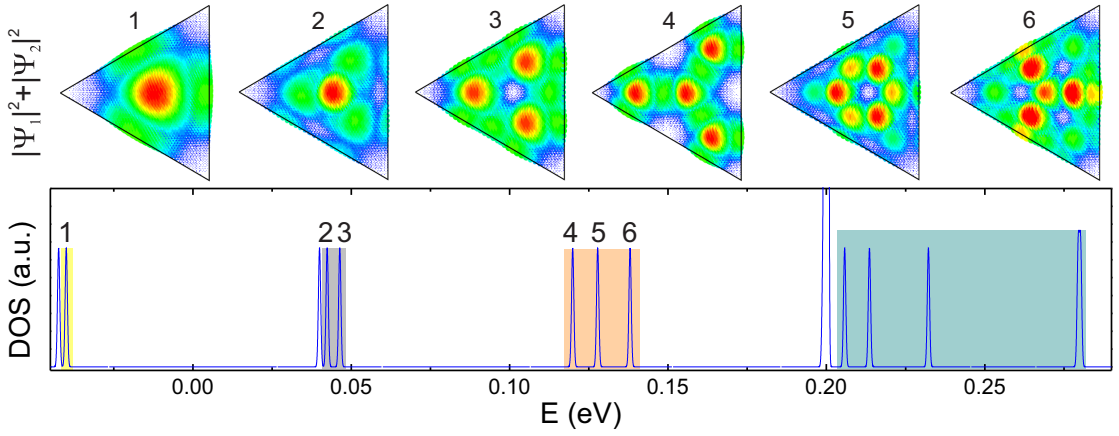

FIG. 13. (Color online) Density of states of triangular AA-stacked bilayer graphene quantum dot with zigzag edges in the absence of an electrostatic bias for $N = 103$ carbon rings on each side, that corresponds to $L \approx 25.415$ nm and $\sqrt{S} \approx 16.724$ nm [see Fig. 12(b)]. The total probability density ($|\Psi_1|^2 + |\Psi_2|^2$) is shown for points 1–6, which belong to the third first groups of states. The different colors on the background of the density of states emphasize the set of states belonging to the same branch. Red (blue) colors represent high (low) amplitude of the wave function.

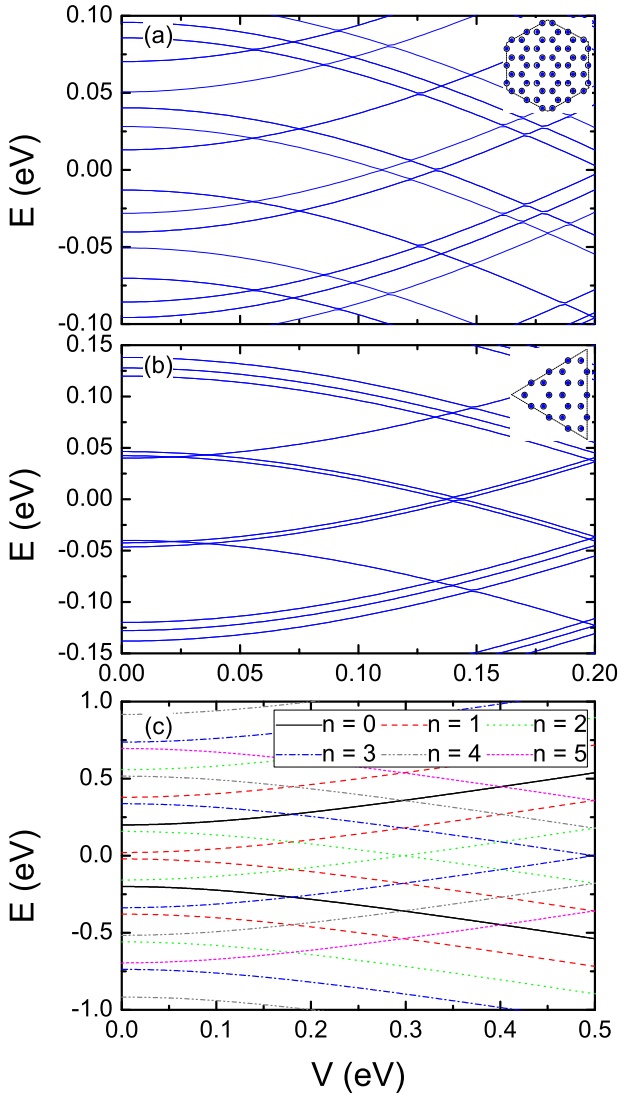

FIG. 14. (Color online) Energy levels as a function of the bias potential V for (a) hexagonal (with $N = 41$ carbon rings in each side, which corresponds to $L \approx 10.084$ nm and $\sqrt{S} \approx 16.254$ nm) and (b) triangular (with $N = 103$ carbon rings in each side, which corresponds to $L \approx 25.415$ nm and $\sqrt{S} \approx 16.724$ nm) AA-stacked BLG QD with zigzag edges. The QD structures are illustrated in the insets. (c) Analytical energy levels [Eq. (4)] obtained from the continuum BLG Hamiltonian as a function of the bias potential V for a fixed size $L = 10.084$ nm for $n \in [0,5]$.

systematically investigated the size and geometry dependence of the energy levels, considering hexagonal and triangular quantum dots. We also analyzed the influence of different types of edges on the electronic structure, by considering bilayer graphene quantum dots terminated with zigzag and armchair edges. A comparison between the results obtained for AA and AB (Bernal) stackings was also presented. For both stacking cases, we compared the energy spectra obtained from the tight-binding approximation to those analytically obtained by the four-band continuum Dirac model, assuming a quantized wave vector $k \propto n\pi/L$, with integer n. Our results showed that the energy levels of bilayer graphene quantum dots depend strongly on the type of geometry and on the type of edge. All degeneracy lifts, gap openings, and electron-hole asymmetries observed in the spectra for biased quantum dots are explained in terms of the breaking of rotational and interlayer symmetries. AB-stacked quantum dots with zigzag edges in the presence of an electrostatic potential exhibit unusual states inside the gap, as predicted by the continuum model, whose nature corresponds to edge confinement. For hexagonal dots, these states are localized at the zigzag edges which are not interlayer connected, and these energy oscillates as either the dot size or the bias potential increases, as a consequence of an interchange between wave function confinement at the edges of the upper and lower layers. For triangular dots, these states stem from the $E = V$ level that penetrates into the gap and resemble the eigenstates of a quantum well along the zigzag edges of the system, whose wave functions exhibit nodes whose number increases as the eigenenergy increases. The energy spectrum for AA-stacked BLG QDs exhibit crossings between electron and hole states for $V = 0$. In contrast to the AB-stacked case, no energy gap is observed for all different geometries and edge types of AA-stacked biased quantum dots studied in this paper, whose energy spectra always preserve the electron-hole symmetry, $E_e = -E_h$.

ACKNOWLEDGMENTS

This work was financially supported by CNPq, under contract NanoBioEstruturas 555183/2005-0, PRONEX/FUNCAP, CAPES Foundation under the process number BEX 7178/13-1, the Flemish Science Foundation (FWO-Vl), the Bilateral programme between CNPq and FWO-Vl, and the Brazilian Program Science Without Borders (CsF).

[1] K. S. Novoselov, A. K. Geim, S. V. Morozov, D. Jiang, Y. Zhang, S. V. Dubonos, I. V. Grigorieva, and A. A. Firsov, Science **306**, 666 (2004).
[2] A. H. Castro Neto, F. Guinea, N. M. R. Peres, K. S. Novoselov, and A. K. Geim, Rev. Mod. Phys. **81**, 109 (2009).
[3] A. V. Rozhkov, G. Giavaras, Y. P. Bliokh, V. Freilikher, and F. Nori, Phys. Rep. **503**, 77 (2011).
[4] B. Trauzettel, D. V. Bulaev, D. Loss, and G. Burkard, Nat. Phys. **3**, 192 (2007).
[5] P. Recher and B. Trauzettel, Nanotechnology **21**, 302001 (2010).
[6] H. P. Heiskanen, M. Manninen, and J. Akola, New J. Phys. **10**, 103015 (2008).
[7] M. Wimmer, A. R. Akhmerov, and F. Guinea, Phys. Rev. B **82**, 045409 (2010).
[8] M. Ezawa, Phys. Rev. B **76**, 245415 (2007).
[9] M. Zarenia, A. Chaves, G. A. Farias, and F. M. Peeters, Phys. Rev. B **84**, 245403 (2011).
[10] M. Grujić, M. Zarenia, A. Chaves, M. Tadić, G. A. Farias, and F. M. Peeters, Phys. Rev. B **84**, 205441 (2011).
[11] E. McCann and M. Koshino, Rep. Prog. Phys. **76**, 056503 (2013).

[12] M. T. Allen, J. Martin, and A. Yacoby, Nat. Commun. **3**, 934 (2012).
[13] A. M. Goossens, S. C. M. Driessen, T. A. Baart, K. Watanabe, T. Taniguchi, and L. M. K. Vandersypen, Nano Lett. **12**, 4656 (2012).
[14] A. Matulis and F. M. Peeters, Phys. Rev. B **77**, 115423 (2008).
[15] P. Recher, J. Nilsson, G. Burkard, and B. Trauzettel, Phys. Rev. B **79**, 085407 (2009).
[16] J. M. Pereira, Jr., P. Vasilopoulos, and F. M. Peeters, Nano Lett. **7**, 946 (2007).
[17] J. M. Pereira, Jr., F. M. Peeters, P. Vasilopoulos, R. N. Costa Filho, and G. A. Farias, Phys. Rev. B **79**, 195403 (2009).
[18] M. Zarenia, B. Partoens, T. Chakraborty, and F. M. Peeters, Phys. Rev. B **88**, 245432 (2013).
[19] A. D. Güçlü, P. Potasz, and P. Hawrylak, Phys. Rev. B **84**, 035425 (2011).
[20] D. Wang, Phys. Lett. A **375**, 4070 (2011).
[21] D. Wang and G. Jin, Phys. Lett. A **377**, 2901 (2013).